Novel Superhard sp^3 Carbon Allotrope from Cold-Compressed C_{70} Peapods

Xigui Yang,[1] Mingguang Yao,[1,*] Xiangying Wu,[1] Shijie Liu,[1] Shuanglong Chen,[1] Ke Yang,[2] Ran Liu,[1] Tian Cui,[1] Bertil Sundqvist,[1,3] and Bingbing Liu[1,†]

[1]State Key Lab of Superhard Materials, Jilin University, Changchun 130012, China
[2]Shanghai Synchrotron Radiation Facilities, Shanghai Institute of Applied Physics, Chinese Academy of Sciences, Shanghai 201204, China
[3]Department of Physics, Umeå University, SE-90187 Umeå, Sweden

(Received 11 May 2016; revised manuscript received 22 December 2016; published 15 June 2017)

Design and synthesis of new carbon allotropes have always been important topics in condensed matter physics and materials science. Here we report a new carbon allotrope, formed from cold-compressed C_{70} peapods, which most likely can be identified with a fully sp^3-bonded monoclinic structure, here named *V* carbon, predicted from our simulation. The simulated x-ray diffraction pattern, near *K*-edge spectroscopy, and phonon spectrum agree well with our experimental data. Theoretical calculations reveal that *V* carbon has a Vickers hardness of 90 GPa and a bulk modulus ~400 GPa, which well explains the "ring crack" left on the diamond anvils by the transformed phase in our experiments. The *V* carbon is thermodynamically stable over a wide pressure range up to 100 GPa, suggesting that once *V* carbon forms, it is stable and can be recovered to ambient conditions. A transition pathway from peapod to *V* carbon has also been suggested. These findings suggest a new strategy for creating new sp^3-hybridized carbon structures by using fullerene@nanotubes carbon precursor containing odd-numbered rings in the structures.

DOI: 10.1103/PhysRevLett.118.245701

Carbon, owing to its flexibility in forming sp^1-, sp^2-, and sp^3-hybridized bonds, exhibits a rich variety of allotropes among which graphite and diamond are the only two major forms existing naturally. The discoveries of fullerenes [1], carbon nanotubes (CNTs) [2], and graphene [3] have spawned intense scientific interest in these materials due to their outstanding properties and diverse potential applications in technology [4–6]. This interest has promoted exploration of novel carbon allotropes from different research fields. Recently, great efforts have been focused on carbon allotropes consisting of all-sp^3-hybridized carbon atoms, and a typical example is the cold compressed post-graphite phase [7]. Similarly, cold compression of CNTs has been reported to produce a possible superhard phase [8]. However, the structures remain elusive so far. Although several candidates [9–16] with distinct topologies have been proposed to explain the mysterious superhard phases, none of them can be unambiguously identified from the experimental x-ray diffraction (XRD) patterns due to the limited number of weak and broad diffraction peaks. Note here that most of the proposed carbon allotropes are constructed from $5+7$ or $4+8$ membered rings [16], while graphite and nanotubes both consist of six-membered rings only. The dissatisfactory match between the theoretical and experimental XRD data in cold compressed graphite and CNTs may indicate a low transformation rate in the conversion of periodic six-membered ring motifs to sp^3 carbon phases constructed from odd $(5+7)$ or even $(4+8)$ carbon rings. A topological consideration suggests to us that a suitable precursor that naturally contains odd-numbered carbon rings (pentagons or heptagons) may have a lower energy barrier to overcome and may thus easier transform into a sp^3 carbon phase at high pressure.

Because fullerenes form closed three-dimensional surfaces, each molecule contains 12 pentagons spatially separated by surrounding hexagons to reduce the steric stress. As typical fullerene molecules, C_{60} or C_{70} can form various polymerized structures when subjected to appropriate pressure and temperature conditions [17,18]. In addition, a new class of structural phases constructed from long-range ordered carbon clusters has been reported by compressing a series of solvated fullerenes [19–21]. Encapsulation of fullerenes such as C_{60} or C_{70} into SWCNTs results in a self-assembled hybrid structure, the so-called peapods [22,23]. As shown in previous work, C_{60} molecules could rotate in SWNTs and exhibit an unusual type of ratcheted rotation under low pressure [24]. Existing results indicate that the fullerenes are quite reactive and easily change their bond type from sp^2 to sp^3 to form new lattice structures under pressure, and thus may be good precursors for new carbon allotropes. Thus, we conceived the idea of creating novel carbon allotropes by compressing peapods, a carbon nanotube-fullerene hybrid structure, naturally containing both pentagons and hexagons.

In this Letter, we demonstrate the synthesis of a highly incompressible carbon allotrope, whose structure most likely has been resolved by our theoretical simulations, from cold compressed C_{70} peapods. Structural predictions were performed using the Crystal Structure Analysis by Particle Swarm Optimization (CALYPSO) algorithm [25,26], which has successfully predicted many other structures at high pressures [9,27–29]. Subsequent structure optimizations and most property calculations were

performed based on the Vienna *ab initio* simulation package (VASP) [30]. Details of the simulations are provided in the Supplemental Material [31].

A C_{70}@SWNT sample was prepared via a vapor-phase method [49]. The diameters of the nanotubes range from 1.3 to 1.5 nm. High pressure experiments were carried out at room temperature, using a diamond anvil cell (DAC) without pressure transmitting medium. Raman measurements were performed using either a Renishaw inVia spectrometer equipped with a 514.5 nm laser or a LabRam HR Evolution spectrometer equipped with 473, 532, and 785 nm lasers. X-ray diffraction data were collected at the BL15U1 beam line of the Shanghai Synchrotron Radiation Facility ($\lambda = 0.6199$ Å) at room temperature. Two-dimensional diffraction patterns were obtained by integrating the two dimensional image with the FIT2D software. For transmission electron microscopy (TEM) and electron energy-loss spectroscopy (EELS) analysis, we used a JEOL JEM-2200FS instrument with an accelerating voltage of 200 kV. The measurements on multiple locations across the samples confirm the spatial homogeneity and validity of the sample. High resolution TEM images of a pristine sample are also shown in Fig. S1 [31].

Figure 1(a) shows the Raman spectra of the peapod samples measured with 785 nm laser excitation under pressure. The spectra recorded at ambient conditions exhibit typical Raman features for C_{70} peapods [50]. Upon compression, the Raman peaks of the C_{70} peapods exhibited the behaviors usually observed, weakened, and disappeared gradually. The G band continuously shifted to higher frequencies and became one broad, weak band at 1670 cm^{-1} at 23 GPa. Above 30 GPa, a broad Raman band emerged in the spectra centered at ~1470 cm^{-1} and became increasingly intense with increasing pressure. This band became asymmetric and the most intense band at pressures higher

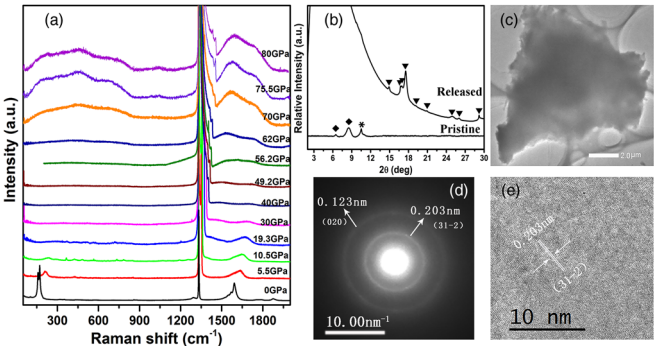

FIG. 1. (a) Raman spectra of C_{70} peapods at selected pressures. The backgrounds of the Raman spectra at pressures above 60 GPa have been carefully subtracted. (b) XRD patterns of the starting material and of samples recovered from 68 GPa. The background of the diffraction pattern of the pristine sample has been carefully subtracted. The peaks marked with rhombus and asterisk represent the diffraction from a two-dimensional triangular lattice and the intertube spacing of SWNTs, respectively. (c) TEM image of the recovered samples. (d) The corresponding SAED pattern. (e) HRTEM image of the recovered samples.

than 60 GPa (upshift to ~1570 cm^{-1}). Additional new peaks can also be observed in the low frequency range (<800 cm^{-1}) and their intensities increase slightly with increasing pressure (see the spectrum at 80 GPa, for example). In earlier literature, other sp^3-rich carbon phases show broad and asymmetric Raman band(s) at ~1500 cm^{-1} and weak bands in the region 300–800 cm^{-1} [51,52]. The similarity between the Raman features of our highly compressed peapods sample and the sp^3 rich carbon phases reported earlier indicates that the compressed peapods transform into a sp^3 rich phase at high pressure.

The XRD patterns of the pristine and recovered samples are shown in Fig. 1(b). The diffraction peaks of the pristine samples at $2\theta = 6.4°$ and 8.5° can be indexed as (30) and (40), respectively, based on a two-dimensional triangular lattice of SWNTs [53]. The peak with a d spacing of 3.382 Å, corresponding to $2\theta = 10.5°$, originates from the intertube spacing of the SWNTs. The XRD patterns of our recovered samples exhibit well-distinguished diffracted peaks (marked with triangles), which differ significantly from those of other carbon phases prepared from cold-compressed graphite, nanotubes, etc. Our experiments on cold compression of pure C_{70} or C_{60} sample showed that both fullerene crystals transformed irreversible into an amorphous phase [54] (see Fig. S2 [31]). To further identify the microstructure of the recovered products in greater detail, we performed TEM in combination with selected area electron diffraction (SAED). Before TEM observation, scanning transmission electron microscopy (STEM) and an energy-dispersive x-ray (EDX) spectroscopy analysis were carried out to ensure that no catalysts (for example, Fe, Ni or other contaminant elements) were present in the recovered products. EDX clearly showed only very small amounts of Si, O, and Cu (see Fig. S3 [31]). Figure 1(c) displays a typical TEM image of the decompressed samples. Electron diffraction patterns [Fig. 1(d)] at multiple regions of the samples turned out to be different from that of a pristine sample shown in Fig. S4 [31], but exhibited reflections with d spacings of 2.028 and 1.224 Å, corresponding to $2\theta = 17.5°$ and 29.2° in the XRD data of the quenched samples. Moreover, the HRTEM image [Fig. 1(e)] clearly shows that the interplanar spacing of about 0.203 nm corresponds to the d value of the diffracted peak at 17.5°, which is also in good agreement with that obtained by SAED. Thus, we conclude that the pristine sample was transformed into a new carbon phase after compression.

Structural simulations were performed in the pressure range of 0–100 GPa to search for the structure of the new phase. Besides the experimentally known cubic and hexagonal diamond and some previously proposed structures, such as M carbon [9], W carbon [12], Z carbon [14] and C carbon [15], we found a novel monoclinic structure with $C2/m$ symmetry (36 atoms/unit cell) [Fig. 2(a)] that we named V carbon. It consists solely of sp^3 bonds and has a five-, six- and seven-membered rings topology pattern, in which two pairs of conjoint five- and seven-membered rings surrounded by six-membered rings are along the b axis.

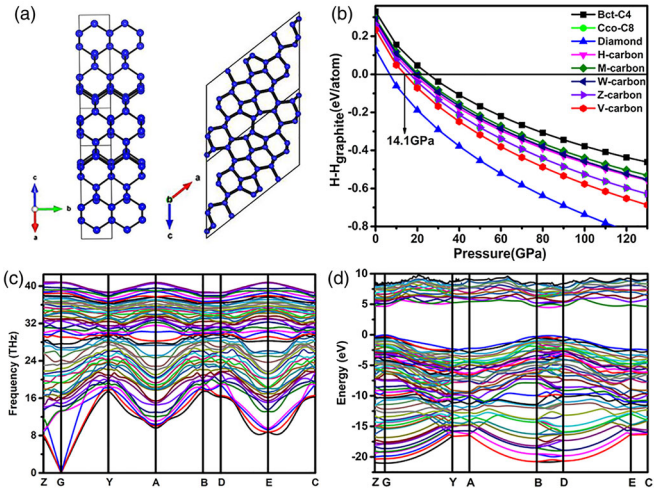

FIG. 2. (a) Predicted *V* carbon structure. (b) Calculated enthalpy per atom for *V* carbon and for previously proposed carbon allotropes versus pressure relative to graphite 2H. (c) Calculated phonon dispersion curves of *V* carbon at 0 GPa. (d) Calculated electronic band structure of *V* carbon at 0 GPa.

More details about the structure are given in Tables S1 and S2 [31], respectively.

To establish the presence of *V* carbon from our experimental observations, we simulated the XRD patterns of *V* carbon and the proposed post-graphite phases and compared with the experimental data in Fig. 3(a). Note that the main characteristics of the *V* carbon are perfectly consistent with our experimental XRD pattern. Five characteristic peaks from the experimental XRD at 14.9°, 16.7°, 16.9°, 17.5°, and 29.2° give satisfactory agreement with the simulated peaks of *V* carbon both in positions and relative intensities. The relatively weaker peaks of *V* carbon at ~19°, ~21°, ~25° and ~26° can explain the experimentally observed shoulder peaks at 19.2°, 20.9°, 25° and 26°, respectively. We further compare our experimental pattern with those of previously proposed structures for the postgraphite phases, and find that only the simulated XRD peaks of *V* carbon match well with our experimental data whereas the peaks from other structures do not. In particular, the strong peak at 17.5° is absent in all other theoretical structures. This suggests that it is very likely that we have correctly identified the structure of the experimentally prepared new phase as *V* carbon.

We also simulated the Raman spectra of *V* carbon at ambient and high pressure to compare with our experimental data. From Figs. S5 and S6 [31] we can see that most of the Raman bands observed under pressure in our experiment are located at or close to those predicted theoretically for *V* carbon. We further made a careful Raman mapping measurement on our quenched product. The obtained Raman spectra show weak Raman bands in the low frequency range from ~300 to 850 cm^{-1}, which is close to the Raman features found from our simulated spectrum. In the high frequency region, very broad bands from 980 to 1600 cm^{-1} can be seen for the quenched sample and this is consistent

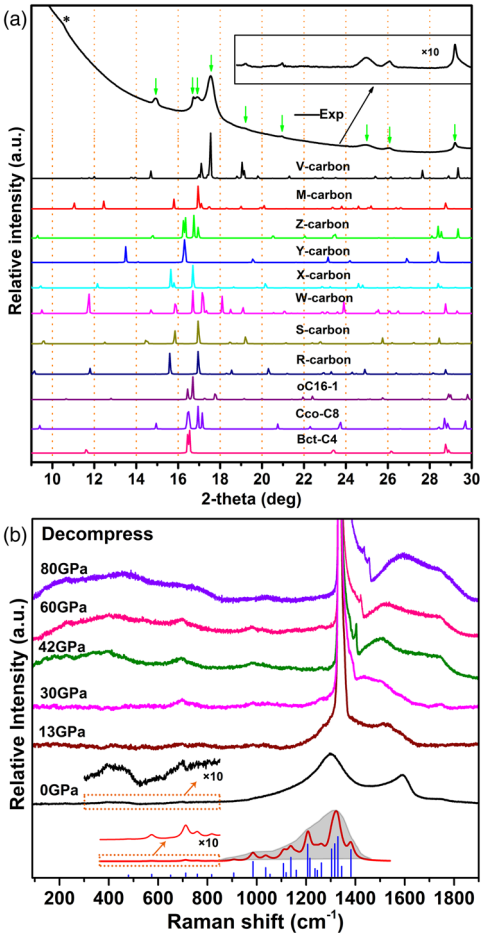

FIG. 3. (a) Simulated XRD patterns of *V* carbon and of previously proposed post-graphite phases compared with our experimental XRD pattern. The asterisk denotes the peak from a graphitelike structure. The experimental new peaks are marked by green arrows. The x-ray wavelength is 0.6199 Å in all cases. (b) Raman spectra of C_{70} peapods upon decompression at pressures as indicated. Simulated Raman spectra of *V* carbon at ambient pressure are shown at the bottom. The computed band profiles with the Lorentzian broadening of 20 cm^{-1} (red line) and 2 cm^{-1} (blue line) are shown for a comparison with the experimental data. The gray shadow is a guideline for the eyes, corresponding to the envelope of the high-frequency Raman-active modes for *V* carbon based on the simulation.

with theoretical predictions that sp^3 carbon structures should exhibit Raman-active modes in this frequency range [Fig. 3(b) and Refs. [55,56]], while the two bands at ~1300 and ~1600 cm^{-1} increase obviously in intensity compared with those at high pressures [see Fig. 3(b)], indicating that the sp^3 bonds formed under pressure might partially transform back to sp^2 bonds. Note that sp^2 sites have a much larger cross section for visible Raman than the sp^3 sites (usually about 50–230 times) [57], and the signals from such sites may thus conceal or overlap with the Raman vibrations from the quenched sp^3 phase, as seen in our spectra. Similar Raman features showing two broad Raman bands in this frequency range have also been observed in other new

carbon phases, for example, a quenched hexagonal carbon phase with a high fraction of sp^3 bonds obtained from cold compressed carbon nanotubes [8] and the postgraphite phase from cold compressed graphite above 15 GPa [7]. Thus, the Raman results are consistent with our XRD measurements, suggesting that the identification of the new phase as *V* carbon is reasonable.

We further calculated the ELNES of *V* carbon to compare with our experimental spectra [Fig. S7 [31]]. The spectrum from recovered samples shows a clear signature of sp^3 carbon with a broad band in the energy range of 290–310 eV ($1s$ to $\sigma*$ transition) [58,59], and a shoulder peak at ~283 eV ($1s$ to $\pi*$ transition). Note that *V* carbon has no $\pi*$ bonding feature, indicating that our recovered samples contain small amounts of sp^2-bonded carbon such as amorphous carbon (*a*-C) or graphite. It is difficult to get accurate component fractions in the recovered samples because of the fact that the EELS spectra are sensitive to the direction of the incident electron beam relative to that of the samples and because of uncertainties in the data processing. Considering a qualitative mixture of graphite/*a*-C and *V* carbon, the $\pi*$ feature can be found in either case and the peaks in the case of graphite/*a*-C and *V* carbon ranging from 320 to 330 eV can reproduce the experimental third broad peak well. Therefore, a small amount of graphitelike or amorphous carbon should be responsible for the weak $\pi*$ peak, which is consistent with our XRD and Raman measurements [Figs. 3(a) and 3(b)]. This result further supports the presence of the predicted *V* carbon structure.

The thermodynamic stability of *V* carbon was examined by a direct enthalpy comparison with known experimental and theoretical carbon allotropes [Fig. 2(b)]. The *V* carbon is energetically more favorable than the structures predicted earlier in the wide pressure range studied, and becomes more stable with respect to graphite 2H at above 14.1 GPa. This suggests that *V* carbon can be achieved under high pressure. We further calculated its phonon dispersion curves from ambient pressure to 100 GPa. Throughout the Brillioun zone [see Fig. 2(c) at zero pressure and Fig. S8 [31] at 100 GPa], the absence of imaginary frequency modes confirms the dynamical stability of *V* carbon. Therefore, once formed, *V* carbon can be quenchable to ambient conditions. In addition, a band structure calculation [Fig. 2(d)] at zero pressure shows that *V* carbon is a wide-gap insulator with an indirect band gap of ~4.48 eV.

The calculated structural properties of *V* carbon at zero pressure and those of other carbon allotropes are given in Table S3 [31]. Interestingly, we can see that the calculated bulk modulus (B_0) and hardness (H_v) of *V* carbon are 411 and 89.4 GPa, respectively. These values are comparable to those of diamond (432, 91.2 GPa) and higher than those of postgraphite carbon phases, indicating that *V* carbon is an ultra-incompressible and superhard material. This provides a reasonable explanation for the observed "ring crack" left on the diamond anvils in our experiment [Fig. S9(a) [31]]. The presence of ring cracks following the original sample boundary in the gaskets after compression has been observed in repeated experiments [Fig. S9(b) [31]]. This is consistent with the case of cracks induced by cold-compressed highly ordered pyrolitic graphite reported recently, for which the formation of a superhard carbon phase was suggested [60]. Other examples of the presence of indentations on diamond anvils due to the formation of superhard phases have also been reported recently [19–21]. We thus suggest that the new phase is a superhard phase, which might be comparable in hardness to that of diamond.

Finally, we present a possible transition route from C_{70} peapods to *V* carbon at an atomistic scale. The formation process from C_{70} peapods to *V* carbon upon compression is shown in Fig. 4 (see the Supplemental Material [31] for details of the calculation). Under pressure, the cross sections of the original tubes change from circular [Fig. 4(a)] to polygonized [Fig. 4(b)]. A further increased pressure then forces the tubes to form a pear-shaped cross section [Fig. 4(c)] due to the support from the hard C_{70} molecules inside the tubes, in agreement with previous simulations [61]. At higher pressure the tubes collapse and distort, and simultaneously, the confined C_{70} deforms following the gradual collapse of the tubes [Figs. 4(d) and 4(e)]. This transformation of C_{70} peapods upon compression is consistent with our experimental observations by Raman spectroscopy. When applying even higher pressure, local distortion and serious collapse of the C_{70} molecules and tubes takes place, driving the breaking of five-membered carbon rings followed by formation of seven-membered carbon rings [Figs. 4(f) and 4(g)], which promotes reconstruction of the molecular structure, connecting atoms via sp^3 bond networks between adjacent tubes and between C_{70} molecules and tubes [Fig. 4(h)], resulting in the formation of the *V* carbon [Fig. 4(i)]. Note that our simulation

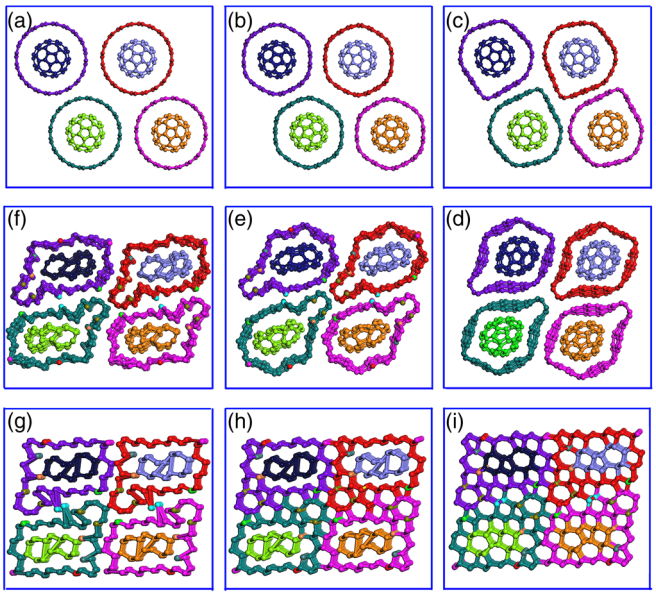

FIG. 4. Transformation pathway of (10,10) CNT bundles with encapsulated C_{70} molecules into the *V* carbon structure under compression.

of compressing a simple mixture of C_{70} and carbon nanotubes calculated by the same method as for C_{70}@SWNTs peapod shows that no *V* carbon was formed [Fig. S10 [31]].

In conclusion, we have created a novel carbon allotrope from cold compressed C_{70} peapods. This new allotrope, can be reasonably identified as a monoclinic structure with atoms connected by fully sp^3-hybridized bonds. This novel carbon structure can be preserved back to ambient conditions and left a ring crack indentation on the diamond anvils. Calculations also revealed *V* carbon to be superhard. Simulated XRD pattern, near *K*-edge spectroscopy, and Raman spectra reproduce well the experimental results. Moreover, a transformation mechanism for C_{70} peapods toward *V* carbon at an atomistic scale has been presented to understand the observed transitions. These results suggest that the intentional inclusion of five-membered carbon rings in the C_{70} peapods starting material facilitates the creation of new structures and establishes the existence of a new carbon allotrope. Our findings may stimulate future studies on the rich structures of carbon using other fullerene@nanotubes carbon precursors containing building blocks based on odd-numbered carbon rings in the structures.

This work was supported financially by the National Natural Science Foundation of China (51320105007, 11634004, 11474121), and the Program for Changjiang Scholars and Innovative Research Team in University (IRT1132). Project No. 2016010 is supported by the Graduate Innovation Fund of Jilin University. We acknowledge R. C. Yu for his helpful discussions and the use of computing facilities at the High Performance Computing Center of Jilin University. We gratefully acknowledge Professor G. T. Zou for his great help.

Note added—.Recently, we were made aware of the existence of the database SACADA [62], listing the structures of all hitherto published allotropes of carbon. We have confirmed that this database does not contain any previous record of the present V structure.

*yaomg@jlu.edu.cn
†liubb@jlu.edu.cn

[1] H. W. Kroto, J. R. Health, S. C. O'Brien, R. F. Curl, and R. E. Smalley, Nature (London) **318**, 162 (1985).
[2] S. Iijima, Nature (London) **354**, 56 (1991).
[3] K. S. Novoselov, A. K. Geim, S. V. Morozov, D. Jiang, Y. Zhang, S. V. Dubonos, I. V. Grigorieva, and A. A. Firsov, Science **306**, 666 (2004).
[4] A. Jorio, G. Dresselhaus, and M. S. Dresselhaus, *Carbon Nanotubes: Advanced Topics in the Synthesis, Structure, Properties and Applications* (Springer Science & Business Media, New York, 2007).
[5] F. Bonaccorso, L. Colombo, G. Yu, M. Stoller, V. Tozzini, A. C. Ferrari, R. S. Ruoff, and V. Pellegrini, Science **347**, 1246501 (2015).
[6] C. N. R. Rao, A. K. Sood, K. S. Subrahmanyam, and A. Govindaraj, Angew. Chem., Int. Ed. **48**, 7752 (2009).
[7] W. L. Mao, H. K. Mao, P. J. Eng, T. P. Trainor, M. Newville, C. C. Kao, D. L. Heinz, J. Shu, Y. Meng, and R. J. Hemley, Science **302**, 425 (2003).
[8] Z. Wang, Y. Zhao, K. Tait, X. Liao, D. Schiferl, C. Zha, R. T. Downs, J. Qian, Y. Zhu, and T. Shen, Proc. Natl. Acad. Sci. U.S.A. **101**, 13699 (2004).
[9] Q. Li, Y. M. Ma, A. R. Oganov, H. B. Wang, H. Wang, Y. Xu, T. Cui, H. K. Mao, and G. T. Zou, Phys. Rev. Lett. **102**, 175506 (2009).
[10] K. Umemoto, R. M. Wentzcovitch, S. Saito, and T. Miyake, Phys. Rev. Lett. **104**, 125504 (2010).
[11] D. Selli, I. A. Baburin, R. Martonak, and S. Leoni, Phys. Rev. B **84**, 161411 (2011).
[12] J.-T. Wang, C. F. Chen, and Y. Kawazoe, Phys. Rev. Lett. **106**, 075501 (2011).
[13] Z. Zhao, B. Xu, X.-F. Zhou, L.-M. Wang, B. Wen, J. He, Z. Liu, H.-T. Wang, and Y. Tian, Phys. Rev. Lett. **107**, 215502 (2011).
[14] M. Amsler, J. A. Flores-Livas, L. Lehtovaara, F. Balima, S. A. Ghasemi, D. Machon, S. Pailhès, A. Willand, D. Caliste, S. Botti, A. S. Miguel, S. Goedecker, and M. A. L. Marques, Phys. Rev. Lett. **108**, 065501 (2012).
[15] D. Li, K. Bao, F. Tian, Z. Zeng, Z. He, B. Liu, and T. Cui, Phys. Chem. Chem. Phys. **14**, 4347 (2012).
[16] H. Niu, X.-Q. Chen, S. Wang, D. Li, W. L. Mao, and Y. Li, Phys. Rev. Lett. **108**, 135501 (2012).
[17] Y. Iwasa, T. Arima, R. M. Fleming, T. Siegrist, O. Zhou, R. C. Haddon, L. J. Rothberg, K. B. Lyons, H. L. Carter, A. F. Hebard, R. Tycko, G. Dabbagh, J. J. Krajewski, G. A. Thomas, and T. Yagi, Science **264**, 1570 (1994).
[18] B. Sundqvist, Adv. Phys. **48**, 1 (1999).
[19] L. Wang, B. Liu, H. Li, W. Yang, Y. Ding, S. V. Sinogeikin, Y. Meng, Z. Liu, X. C. Zeng, and W. L. Mao, Science **337**, 825 (2012).
[20] W. Cui, M. Yao, S. Liu, F. Ma, Q. Li, R. Liu, B. Liu, B. Zou, T. Cui, and B. Liu, Adv. Mater. **26**, 7257 (2014).
[21] M. Yao, W. Cui, M. Du, J. Xiao, X. Yang, S. Liu, R. Liu, F. Wang, T. Cui, B. Sundqvist, and B. Liu, Adv. Mater. **27**, 3962 (2015).
[22] B. W. Smith, M. Monthioux, and D. E. Luzzi, Nature (London) **396**, 323 (1998).
[23] C. Caillier, D. Machon, A. San-Miguel, R. Arenal, G. Montagnac, H. Cardon, M. Kalbac, M. Zukalova, and L. Kavan, Phys. Rev. B **77**, 125418 (2008).
[24] Y. Zou, B. Liu, L. Wang, D. Liu, S. Yu, P. Wang, T. Wang, M. Yao, Q. Li, B. Zou, T. Cui, G. Zou, T. Wågberg, B. Sundqvist, and H.-K. Mao, Proc. Natl. Acad. Sci. U.S.A. **106**, 22135 (2009).
[25] Y. Wang, J. Lv, L. Zhu, and Y. Ma, Phys. Rev. B **82**, 094116 (2010).
[26] Y. Wang, J. Lv, L. Zhu, and Y. Ma, Comput. Phys. Commun. **183**, 2063 (2012).
[27] J. Lv, Y. Wang, L. Zhu, and Y. Ma, Phys. Rev. Lett. **106**, 015503 (2011).
[28] Q. Li, D. Zhou, W. Zheng, Y. Ma, and C. Chen, Phys. Rev. Lett. **110**, 136403 (2013).
[29] Y. Li, J. Hao, H. Liu, S. Lu, and J. S. Tse, Phys. Rev. Lett. **115**, 105502 (2015).

[30] G. Kresse and J. Furthmüller, Phys. Rev. B **54**, 11169 (1996).
[31] See Supplemental Material at http://link.aps.org/supplemental/10.1103/PhysRevLett.118.245701 for calculation methods, lattice parameters, bulk modulus, hardness, phonon dispersion, HRTEM images of C_{70} peapods, x-ray diffractions of the starting and recovered C_{70} and C_{60} sample from high pressure, comparison of simulated and experimental Raman spectra under high pressure, EELS spectra of recovered samples, optical images of diamond anvils, and the transformation process of compressing a simple mixture of C_{70} and carbon nanotubes under pressure, which includes Refs. [32–48].
[32] J. P. Perdew, K. Burke, and M. Ernzerhof, Phys. Rev. Lett. **77**, 3865 (1996).
[33] P. E. Blochl, Phys. Rev. B **50**, 17953 (1994).
[34] G. Kresse and D. Joubert, Phys. Rev. B **59**, 1758 (1999).
[35] M. D. Segall, P. J. M. Lindan, M. J. Probert, C. J. Pickard, P. J. Hasnip, S. J. Clark, and M. C. Payne, J. Phys. Condens. Matter **14**, 2717 (2002).
[36] A. Togo, F. Oba, and I. Tanaka, Phys. Rev. B **78**, 134106 (2008).
[37] R. Hill, Proc. Phys. Soc. London Sect. A **65**, 349 (1952).
[38] K. Li, X. Wang, F. Zhang, and D. Xue, Phys. Rev. Lett. **100**, 235504 (2008).
[39] http://accelrys.com/products/materials-studio/modules/forcite.html.
[40] S. B. Legoas, V. R. Coluci, S. F. Braga, P. Z. Coura, S. O. Dantas, and D. S. Galvao, Phys. Rev. Lett. **90**, 055504 (2003).
[41] K. S. Troche, V. R. Coluci, S. F. Braga, D. D. Chinellato, F. Sato, S. B. Legoas, R. Rurali, and D. S. Galvao, Nano Lett. **5**, 349 (2005).
[42] A. K. Rappe, C. J. Casewit, K. S. Colwell, W. A. Goddard, and W. M. Skiff, J. Am. Chem. Soc. **114**, 10024 (1992).
[43] D. Root, C. Landis, and T. Cleveland, J. Am. Chem. Soc. **115**, 4201 (1993).
[44] S. Nose, J. Chem. Phys. **81**, 511 (1984).
[45] Z. Li, F. Gao, and Z. Xu, Phys. Rev. B **85**, 144115 (2012).
[46] X. L. Sheng, Q. B. Yan, F. Ye, Q. R. Zheng, and G. Su, Phys. Rev. Lett. **106**, 155703 (2011).
[47] H. J. Mcskimin, P. Andreatch, Jr., and P. Glynn, J. Appl. Phys. **43**, 985 (1972).
[48] F. Occelli, P. Loubeyre, and R. Letoullec, Nat. Mater. **2**, 151 (2003).
[49] H. Kataura, Y. Maniwa, M. Abe, A. Fujiwara, T. Kodama, K. Kikuchi, H. Imahori, Y. Misaki, S. Suzuki, and Y. Achiba, Appl. Phys. A **74**, 349 (2002).
[50] P. M. Rafailov, C. Thomsen, and H. Kataura, Phys. Rev. B **68**, 193411 (2003).
[51] A. C. Ferrari and J. Robertson, Phys. Rev. B **64**, 075414 (2001).
[52] M. Yao, V. Pischedda, B. Sundqvist, T. Wagberg, M. Mezouar, R. Debord, and A. S. Miguel, Phys. Rev. B **84**, 144106 (2011).
[53] G. Liu, Y. Zhao, K. Deng, Z. Liu, W. Chu, J. Chen, Y. Yang, K. Zheng, H. Huang, W. Ma, L. Song, H. Yang, C. Gu, G. Rao, C. Wang, S. Xie, and L. Sun, Nano Lett. **8**, 1071 (2008).
[54] J. R. Patterson, S. A. Catledge, and Y. K. Vohra, Appl. Phys. Lett. **77**, 851 (2000).
[55] J. A. Flores-Livas, L. Lehtovaara, M. Amsler, S. Goedecker, S. Pailhès, S. Botti, A. S. Miguel, and M. A. L. Marques, Phys. Rev. B **85**, 155428 (2012).
[56] Y. Bai, X. Zhao, T. Li, Z. Lv, S. Lv, H. Han, Y. Yin, and H. Wang, Carbon **78**, 70 (2014).
[57] A. C. Ferrari and J. Robertson, Phys. Rev. B **63**, 121405 (2001).
[58] R. Arenal, P. Bruno, D. J. Miller, M. Bleuel, J. Lal, and D. M. Gruen, Phys. Rev. B **75**, 195431 (2007).
[59] I. Konyashin, A. Zern, J. Mayer, F. Aldinger, V. Babaev, V. Khvostov, and M. Guseva, Diam. Relat. Mater. **10**, 99 (2001).
[60] Y. Wang, J. E. Panzik, B. Kiefer, and K. K. M. Lee, Sci. Rep. **2**, 520 (2012).
[61] N. M. Pugno and J. A. Elliott, Physica E (Amsterdam) **44**, 944 (2012).
[62] R. Hoffmann, A. A. Kabanov, A. A. Golov, and D. M. Proserpio, Angew. Chem., Int. Ed. **55**, 10962 (2016).